View Article Online / Journal Homepage / Table of Contents for this issue
Dynamic Article Links

Soft Matter

Cite this: *Soft Matter*, 2012, **8**, 2965

www.rsc.org/softmatter

PAPER

High-fidelity fabrication of Au–polymer Janus nanoparticles using a solution template approach†

Tingling Rao,[a] Xue-Hui Dong,[a] Byran C. Katzenmeyer,[b] Chrys Wesdemiotis,[b] Stephen Z. D. Cheng[a] and Matthew L. Becker*[ac]

Received 19th October 2011, Accepted 6th January 2012
DOI: 10.1039/c2sm07002b

Published on 02 February 2012. Downloaded by University of Akron on 02/02/2015 19:01:47.

Janus particles have attracted significant attention in recent years, due to their potential in nanomanufacturing. Their asymmetric features impart unique physical and chemical properties, which can be tuned and utilized to control their solution-state assembly. While several examples of Janus nanostructures have been reported in the literature, the scientific community continues to pursue synthetic routes which are less time and resource intensive. Herein, we describe a facile method to synthesize Janus nanoparticles in which colloidal micelles template the *in situ* formation of Au nanoparticles in the shell layer. The resulting morphologies of the hybrid Au–polymer nanoparticles can be adjusted widely by controlling the polymer and reducing agent (HEPES (4-(2-hydroxyethyl)-1-piperazineethanesulfonic acid)) concentrations. High-fidelity populations of Au–micelle Janus nanoparticles are obtained when the polymer concentration is high ($\geq 1.0 \times 10^{-6}$ mmol L^{-1}) and the HEPES concentration is low (≤ 0.3 mol L^{-1}). Conversely, when the HEPES concentration is high (≥ 0.5 mol L^{-1}) and the polymer concentration is low ($\leq 2.4 \times 10^{-7}$ mmol L^{-1}), raspberry-like clusters are formed, where each micelle encumbers several Au nanocrystals. Our method is attractive in that the number of Au nanoparticles on each Au–micelle entity can be controlled using a scalable, aqueous solution process. It also has significant potential for the directed assembly of Au nanoparticle superstructures, as the nature and geometry of the polymer precursors can be varied.

Introduction

Since De Gennes introduced the concept of "Janus Grains", named after the mythological figure Janus who possessed two distinct faces, efforts to synthesize anisotropic Janus particles have been pursued widely with varying levels of success.[1–3] With well-defined structures and asymmetric interfacial interactions, Janus particles exhibit novel physical and chemical properties, which provides new opportunities in the fabrication of optical probes,[4,5] sensing devices,[6,7] phase-transfer catalysts,[8,9] and drug carriers.[10–12] Significantly, Janus particles mimic at a very simple level Nature's ability to facially and regioselectively functionalize materials and further to selectively assemble these materials into hierarchical structures which afford complex functionalities.[13] Many efforts have been devoted to synthesizing asymmetric, hybrid particles. General approaches have included template-assisted synthesis,[14–17] self-assembly of polymer,[18,19] microfluidic techniques,[20] selective surface modification[21] and surface nucleation.[22–24] Additional efforts have focused on simplifying the respective fabrication processes and scaling the fabrication such that usable quantities are generated for nanomanufacturing. So as facile and robust approaches to synthesize Janus particles yield larger quantities of well-defined materials,[25–28] the demand for highly functional advanced materials will increase.

Among the various types of Janus particles, asymmetric inorganic–organic hybrid nanoparticles are especially interesting. Colloidal particles such as micelles formed by amphiphilic block polymer self-assembly present a variety of morphologies, which can be tuned by varying block compositions, molecular weight, solvent properties, block copolymer concentrations, *etc.*[29–32] Increased stability compared with small molecular surfactants has also proved useful in medical and biological applications.[33] Recently, inorganic nanoparticles, especially Au clusters, have attracted interest in molecular imaging probes,[34,35] gene therapy[36] and catalysis.[37] Advances in the development of synthetic routes and methodologies to make organic–inorganic hybrid materials with novel multi-functional nanostructures have enabled fundamental and applied investigations of the size, shape, and packing dependent properties.[38–41] However, due to the symmetrical shape and isometric composition of nanoparticles, it is still difficult to

[a]*Department of Polymer Science, The University of Akron, Akron, OH 44325-3909, USA. E-mail: becker@uakron.edu; Fax: +1 330-972-5290; Tel: +1 330-972-2834*
[b]*Department of Chemistry, The University of Akron, Akron, OH 44325, USA*
[c]*Center for Biomaterials in Medicine, Austen Bioinnovation Institute in Akron, Akron, OH 44308, USA*

† Electronic supplementary information (ESI) available: Quantitative data from SEM pictures and ESI-MS ionization experiments. See DOI: 10.1039/c2sm07002b

View Article Online

Published on 02 February 2012. Downloaded by University of Akron on 02/02/2015 19:01:47.

synthesize hybrid nanoparticles with a defined stoichiometry. Herein, we report a facile and novel method to synthesize well-defined populations of asymmetric, hybrid Au–polymer Janus nanoparticles possessing Au nanoparticles grown directly from within the coronas of the micelles.

Experimental section

Materials

The following chemicals were used as received: gold(III) chloride hydrate ($HAuCl_4$, Aldrich, 99.999%), 4-(2-hydroxyethyl)-1-piperazineethanesulfonic acid (HEPES, Aldrich, ≥99.5%), *N*,*N*-dimethylformamide anhydrate (DMF, Aldrich, 99.8%), sodium azide (NaN_3, Aldrich, ReagentPlus®, >99.5%), epichlorohydrin (Acros, 99%), *N*,*N*-dimethylformamide (DMF, Aldrich 99.9%), methanol (MeOH, Fisher Scientific, reagent grade), deuterated chloroform ($CDCl_3$ Aldrich, 99.8 atom% D), *N*,*N*,*N*′,*N*″,*N*″-pentamethyldiethylenetriamine (PMDETA, Aldrich, 99%), triethylamine (TEA, Aldrich, 99%), 2-bromoisobutyryl bromide (Aldrich, 98%), ammonium chloride (NH_4Cl, Aldrich, >99.5%), and sodium hydroxide (NaOH, Aldrich, ≥97.0%). Cuprous bromide (CuBr, Aldrich, 98%) was freshly purified by stirring in acetic acid overnight, washed with acetone, and dried in a vacuum. Dichloromethane (CH_2Cl_2, Fisher Scientific, reagent grade) and styrene (Aldrich, 99%) were purified by stirring over freshly ground calcium hydride for 12 h and redistilled under vacuum before use.

Block polymer synthesis

The PEO precursor was purchased from Polymer Source (M_n = 10.0 kg mol^{-1}, M_w = 10.6 kg mol^{-1}, PDI = 1.06). The PEO-*b*-PS diblock copolymer was synthesized according to previously described methods.[41] The homo- and block copolymers were characterized by size exclusion chromatography (SEC, polystyrene standards) and ^{1}H nuclear magnetic resonance (^{1}H NMR). The block copolymer was measured to have a number average molecular weight (M_n, overall) of 56 kg mol^{-1}, and a weight-average molecular weight (M_w, overall) of 60 kg mol^{-1}. The polydispersity (PDI) was measured to be 1.07 according to SEC chromatography. The molecular weight of PS block can be calculated to be 46 kg mol^{-1}. Volume fractions of the PEO and PS block are 17.9% and 82.1% respectively.

Micelle formation

PEO-*b*-PS (10 mg) was dissolved in 10 mL pre-filtered anhydrous DMF to obtain a 0.1 wt% stock solution. It was stirred at room temperature for 24 h to ensure that the polymer was completely dissolved. Ultrapure water (18 MΩ cm^{-1}) was added dropwise into the solution. Each drop added was ~0.1 wt% water of the total solution weight, and at least a 15 min gap was maintained between two consecutive drops. The final water content was 4.76%. Then solution was sealed and left to stir overnight before dialysis.

Equipment

UV-Vis spectra were recorded on a HP 8453 UV-Vis Spectrometer System with a resolution of 2 nm. Dynamic light scattering experiments were conducted using a Brookhaven Instrument coupled to a BI-200SM goniometer, a BI-9000AT correlator, and an EMI-9863 photomultiplier tube for photon counting. A Meller Griot 35 mW He–Ne laser was used as the light source (632.8 nm). A cylindrical glass scattering cell with a diameter of 12 mm was placed at the center of a thermostat bath (0.01 °C) with decahydronaphthalene used for refractive index matching. The solutions were filtered into the scattering cells through syringe filters of 0.45 or 1.0 μm pore size. Both the scattering intensity and hydrodynamic diameter were measured at a scattering angle of 90° at 25 °C. The measurement was repeated 3 times and with collection times of 30 min. Average counts were 157.2 kcp. CONTIN analysis with measured baseline was used to determine the distributions. Bright field transmission electron microscopy (TEM) images were recorded in a JEOL-1230 microscope with an accelerating voltage of 120 kV. 3 μL of the Au–micelle solutions were deposited onto copper grids. After ~3 min, the excess solution was wicked away by a piece of filter paper. The sample was then allowed to dry under ambient conditions. TEM images were recorded on a digital CCD camera and processed with the accessory digital imaging system. Micelle and Au nanoparticle sizes were measured with the digital imaging software "Image Tool". Numbers of Au nanoparticles on each micelle were counted directly through TEM images. And for each condition, more than 500 nanoparticles were counted for particle counting statistics based on more than 30 TEM images. Blank micelles and micelle–Au aggregates were not taken into account. Electrospray ionization mass spectrometry (ESI-MS) data were collected using a Bruker HCT Ultra II quadrupole ion-trap (QIT) mass spectrometer (Bruker Daltonics, Billerica, MA). Samples were dissolved in methanol/water (20%, v/v). Sample solutions were introduced by direct infusion into the instrument at a rate of 360 μL h^{-1} using a syringe pump. A potential of +4.0 kV (negative ion mode) was applied to the entrance of the sampling capillary, which is orthogonal to the grounded spraying needle. Nitrogen was used as the nebulizing gas (10 psi), which flows coaxially with the spray and aids in the formation of charged droplets, and as the drying gas (8 L min^{-1}, 300 °C), which heats the sampling capillary to help in the droplet desolvation process. Ions were allowed to accumulate up to a maximum time of 200 ms before mass-selective ejection through ramping up of the RF potential of the ring electrode for *m*/*z* measurement. All quoted *m*/*z* values are monoisotopic.

Scheme 1 summarizes the procedures we utilized to obtain gold–polymer Janus nanoparticles. In our method, the amphiphilic block copolymer PEO-*b*-PS was utilized to form micelles. The PEO corona accumulates and sequesters locally $AuCl_4^-$ ions. The formation of inorganic–organic hybrid nanoparticles occurs *via in situ* reduction of $HAuCl_4$ into Au nanoparticles. Through careful adjustment of both the reducing agent as well as micelle template concentrations, we were able to obtain Au–micelle Janus nanoparticles as a nearly monodisperse product.

The PEO-*b*-PS polymer precursor was synthesized as described previously.[42] The molecular characteristics of the block copolymer and the precursor were determined by size exclusion chromatography (SEC) and the data are summarized in Table 1. Additional details are described in the ESI†.

 This journal is © The Royal Society of Chemistry 2012

View Article Online

Published on 02 February 2012. Downloaded by University of Akron on 02/02/2015 19:01:47.

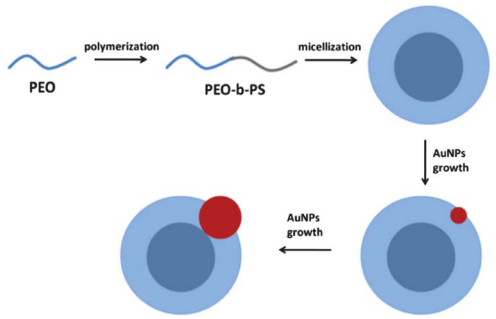

Scheme 1 Schematic illustration of the process to generate Au–micelle asymmetric nanoparticles.

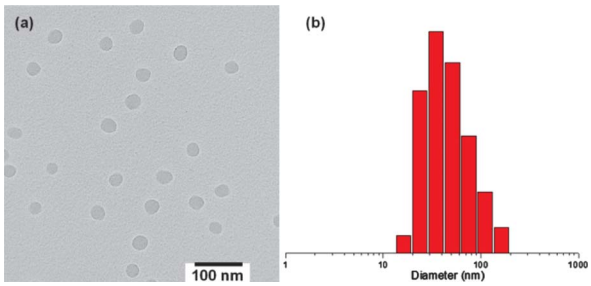

Fig. 1 (a) Bright field TEM image of PEO-*b*-PS micelle precursors; and (b) hydrodynamic radius, D_h, measured by dynamic light scattering (intensity average) shows a nearly monodisperse micelle population with the average size measuring 40 nm.

PS-*b*-PEO is an amphiphilic copolymer, which self-assembles into narrow polydispersity core–shell micelles in aqueous solution under the appropriate conditions. Details of the thermodynamics have been discussed and reviewed previously.[43–45] To prepare spherical micelles, PEO_{227}-*b*-PS_{442} was first dissolved in pre-filtered anhydrous DMF *via* stirring at room temperature for at least 24 h to obtain a 0.1 wt% stock solution. Water was chosen as the selective solvent for the PEO block. Ultrapure water (18 MΩ cm^{-1}) was added drop wise to 10 mL of a stock solution (0.1 wt%) to reach a predetermined water and DMF ratio (1 : 20). Water was added slowly (rate ~40 μL h^{-1}) in order for the solution to reach the thermodynamic equilibrium.

After the solution reached equilibrium, it was quickly quenched in a large amount of water and dialyzed for 2 days in a 500–1000 Da molecular weight cutoff (MWCO) tubing (Spectrum Laboratories, Inc., Rancho Domingo, CA) before lyophilization. Fig. 1a shows a representative bright field TEM image of spherical micelles of PEO_{227}-*b*-PS_{442} from DMF/water solution with a water concentration of ~4.76%. The average diameter of the spherical micelles was measured to be ~30 nm with a relatively narrow size distribution. Fig. 1b shows the hydrodynamic diameter, D_h, and distribution of the micelles was measured utilizing dynamic light scattering (DLS). It indicates that the average diameter is about 40 nm, which is larger than the TEM results due to the collapse of corona after drying and the scattering from the highly hydrated shell chains in solution.

To facilitate Janus particle formation, dialyzed micelles were resuspended and diluted into stock solution with HEPES buffer at several different predetermined concentrations. Then a stock solution (2.45 mmol L^{-1}) of chloroauric acid ($HAuCl_4$) was added (300 μL) to 700 μL of each prepared micelle HEPES solution to yield a final concentration of 0.735 mmol L^{-1}. From the master mix, aliquots were divided into 4 groups according to differing HEPES concentrations, 0.1 mol L^{-1}, 0.3 mol L^{-1}, 0.5 mol L^{-1} and 0.7 mol L^{-1}, respectively. Within each HEPES concentration, 4 different polymer concentrations were subdivided. The final diblock copolymer concentrations were identical for each of the 0.1 mol L^{-1} and 0.3 mol L^{-1} HEPES samples, which ranged from 2.0×10^{-7} mol L^{-1} to 1.4×10^{-6} mol L^{-1}. The polymer concentration was lower for the higher HEPES concentration samples (0.5 mol L^{-1} and 0.7 mol L^{-1}), which ranged from 8.0×10^{-8} mol L^{-1} to 5.6×10^{-7} mol L^{-1}. We have found that when the HEPES concentration is too high (>0.7 mol L^{-1}), the micelle stability is strongly affected. The micelles disassemble as the HEPES concentration increased beyond this threshold. However, if the concentration of micelles remains below the critical value for each set of experiments within a specific HEPES concentration, the micelles gradually lose the ability to sequester sufficient amounts of gold salts for controlling the resulting morphologies of Au nanoparticles. The composition information for each reaction system is shown in Table 2.

In our method, the Au–micelle hybrid morphologies are controlled by varying both the concentration of HEPES and micelles, which is mainly the volume fraction of PEO in solution. HEPES plays an active chemical role as the reducing agent of the Au^{3+} salts, of which the concentration strongly affects the rate of nucleation and crystal growth, and further affects the size and morphology of Au nanoparticles. The micelle coronas are functioning as templates, in which the Au^{3+} salts are accumulating preferentially due to the dative bonding effect of the PEO chains. The locally concentrated PEO chains are able to form pseudo-crown ether cavities, which can bind $AuCl_4^-$ ions and further aid in the formation of the Au nanocrystals in the presence of reducing agent. It has been reported previously that PEO with molecular weights larger than 1.45 kDa will accumulate Au salts within the corona layer similar to a crown ether solubiliziation effect observed with other cations.[46] Upon the

Table 1 Molecular characterization of block polymer

Polymer	M_n[a]/Da	M_w[a]/Da	M_w/M_n[a]	N_{PEO}[b]	N_{PS}[b]	Φ_{PEO}[c]	Φ_{PS}[c]
PEO	10 000	10 600	1.06	227	—	—	—
PEO-*b*-PS	56 000	60 000	1.07	227	442	17.9%	82.1%

[a] Molecular weight and molecular weight distribution were measured by SEC. [b] Degree of polymerization, N, was calculated based on the equation: N = (total M_w of polymer)/(M_w of monomer unit) = M_n/M_0. [c] Volume fraction was calculated based on the equation: Φ = (volume of polymer block)/(total volume of copolymer) = $V_{(A)}/V_{(total)}$.

View Article Online

Published on 02 February 2012. Downloaded by University of Akron on 02/02/2015 19:01:47.

Table 2 Reaction recipes at a constant $HAuCl_4$ concentration (0.735 mmol L^{-1})

HEPES 0.1 mol L^{-1}	[Polymer]/mol L^{-1}	HEPES 0.3 mol L^{-1}	[Polymer]/mol L^{-1}	HEPES 0.5 mol L^{-1}	[Polymer]/ mol L^{-1}	HEPES 0.7 mol L^{-1}	[Polymer]/mol L^{-1}
1a	1.4×10^{-6}	2a	1.4×10^{-6}	3a	5.6×10^{-7}	4a	5.6×10^{-7}
1b	1.0×10^{-6}	2b	1.0×10^{-6}	3b	4.0×10^{-7}	4b	4.0×10^{-7}
1c	6.0×10^{-7}	2c	6.0×10^{-7}	3c	2.4×10^{-7}	4c	2.4×10^{-7}
1d	2.0×10^{-7}	2d	2.0×10^{-7}	3d	8.0×10^{-8}	4d	8.0×10^{-8}

introduction of a reducing agent, the complexes yield Au nanoparticles in water under mild conditions.[46–48]

We have confirmed the preferential accumulation of Au salts in the micelles using electrospray ionization mass spectrometry (ESI-MS). Using a set of sequential experiments, we measured the ion concentration of Au in a master aqueous solution (0.735 mmol L^{-1}). A separate aliquot was made in which micelles ([polymer] = 1.0×10^{-6} and [$HAuCl_4$] = 0.735 mmol L^{-1}) were deposited. Another solution was made with the same polymer and $HAuCl_4$ concentration but in 0.3 mol L^{-1} HEPES buffer. After being allowed to react, the last two solutions were each split into two aliquots, one of which was centrifuged. Each of the five solutions was then assessed using ESI-MS to measure the Au concentration present in solution. The solution concentration of gold was reduced drastically (from 352 523 (arbitrary units) in the master mix to 58 984 in the micelle solution to 4930 in the reduced supernatant) in a step-wise fashion. The individual spectra are presented in the ESI†.

Taking advantage and extending this synthetic method, we modified the morphology of PEO into narrowly dispersed spheres using well-defined block copolymer precursors. The block copolymer micelles function as templates for *in situ* growth of Au nanoparticles. The concentration of micelles also has a strong impact on morphologies of the hybrid nanoparticles. Under the same HEPES buffer conditions, as the micelle concentration increases, the number of nucleation sites on each micelle sphere will decrease.

Fig. 2a–d show statistical histograms representing distributions of numbers of Au nanoparticles per micelle as a function of the fabrication procedures according to Table 2. For each reaction condition, more than 500 particles were counted (see Fig. S7–S10 in the ESI† for the representative bright field TEM images used to generate the histogram). Within each plot, the highest production of Au–micelle Janus particles occurs when micelles are most concentrated, of which, the maximum is present in component 2a in Fig. 2b for all 16 recipes. In Fig. 2a and b, under each reaction condition, the overall portion of Au–micelle hybrids is decreasing as the number of Au nanoparticles per micelle increases. A transition occurs in Fig. 2c. Within the plot, from column 3c, the distribution of the number of AuNPs on each micelle is shifted to a higher level with a sudden drop of Au–micelle Janus hybrids production. The shift becomes more apparent as the HEPES concentration is further increased. In Fig. 2d, the possibility to show Janus morphology is sacrificed. In columns 4c and 4d, majority of the hybrids shows 3 to 5 AuNPs on each micelle.

To clearly demonstrate the effect of reaction conditions on the transition tendency of the Janus particle fraction, Fig. 3a shows the Janus nanoparticle percentages of all 16 recipes as a function of HEPES and block copolymer concentrations generated from Fig. 2. Fig. 3a shows the transition tendency of the Janus particle heterogeneity fraction according to variations in HEPES and

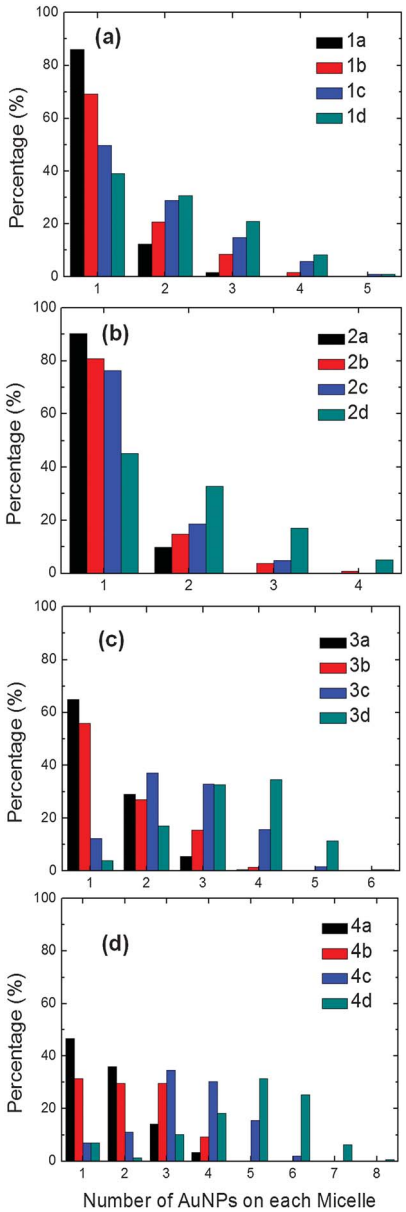

Fig. 2 (a–d) Statistical histograms depict the number of AuNPs located on each micelle for all 16 reaction conditions listed in Table 2. (a) 0.1 mol L^{-1} HEPES; (b) 0.3 mol L^{-1} HEPES; (c) 0.5 mol L^{-1} HEPES; and (d) 0.7 mol L^{-1} HEPES.

 This journal is © The Royal Society of Chemistry 2012

View Article Online

Published on 02 February 2012. Downloaded by University of Akron on 02/02/2015 19:01:47.

block copolymer concentrations. For each column, more than 500 particles were counted (see Fig. S3–S6 in the ESI† for the representative bright field TEM images used to get the histogram). In Fig. 3a, the *z*-axis represents the overall portion of Au–micelle Janus morphologies in the hybrid nanoparticle population. The *x*- and *y*-axes indicate the extent to which the hybrid morphologies are simultaneously affected by HEPES and polymer concentrations, respectively. For each set of columns with the same HEPES value, the percentage of Janus particles within the population is decreasing as micelles become more and more dilute. Concentrated micelle solutions ($\geq 1.0 \times 10^{-6}$ mol L^{-1}) with low HEPES concentrations (0.1 mol L^{-1} and 0.3 mol L^{-1}) are able to host the growth of high-fidelity Au–micelle Janus particles. The optimal conditions (~90%) for Janus particle formation are 0.3 mol L^{-1} HEPES and 1.4×10^{-6} mol L^{-1} polymer (Table 2, 2a).

The instability of micelles in concentrated HEPES solution has limited the comparison of the effect of micelle concentrations with the same reducing agent. However, in the dilute micelle regime ($\leq 2.4 \times 10^{-7}$ mol L^{-1}), the blue columns indicate that with concentrated HEPES (0.5 mol L^{-1} and 0.7 mol L^{-1}), the Janus nanoparticles fraction is directly reduced to less than 20%. Fig. 3b shows a bright field TEM image of the Au–micelle hybrid with highest Janus nanoparticles occupation (Table 2, 2a). The bifunctional nanoparticles show distinct Janus morphology, with the micelles diameter averaging 30 nm and Au approximately 10 nm. The Au nanoparticles appear black and micelles are light colored in the image because of the higher electron density of Au particle, which prevents transmission of the electrons. Fig. 3c shows bright field TEM images of the Au–micelles hybrid synthesized with low micelle but high HEPES concentration (Table 2, 4d). Each micelle is coupled with multiple Au nanoparticles with diameters around 20 nm which present raspberry-like morphology. Statistical diagrams for the portion of the ratio of Au nanoparticles/micelles are shown in the ESI†.

In order to investigate the effect of polymer and HEPES concentrations on the nanocrystals, UV-Vis absorbance was measured for each of the 16 conditions. The Au nanocrystal absorbance spectrum is dominated by a characteristic surface plasmon resonance (SPR) peak, of which the details have been discussed and reviewed.[48–51] The nanocrystal SPR peak appears as a broad absorbance band centered near a wavelength of 520–530 nm when the size of Au cluster exceeds 1.5 nm. The SPR maximum wavelength λ_{max} deviates depending on particle size, shape, dielectric constant and temperature. Fig. 4a shows the λ_{max} shift of Au nanocrystals with several polymer and HEPES concentrations. Each point represents the average of three independent UV-Vis measurements. Increasing the polymer concentration will result in a reduction in the amount of available gold particles on each micelle sphere. The blue shift of λ_{max} when keeping HEPES constant confirms that the particle size is getting smaller as the micelle content is increasing. The HEPES concentration also has a strong impact on SPR of Au nanocrystals. It has been reported that the amount of reducing agent

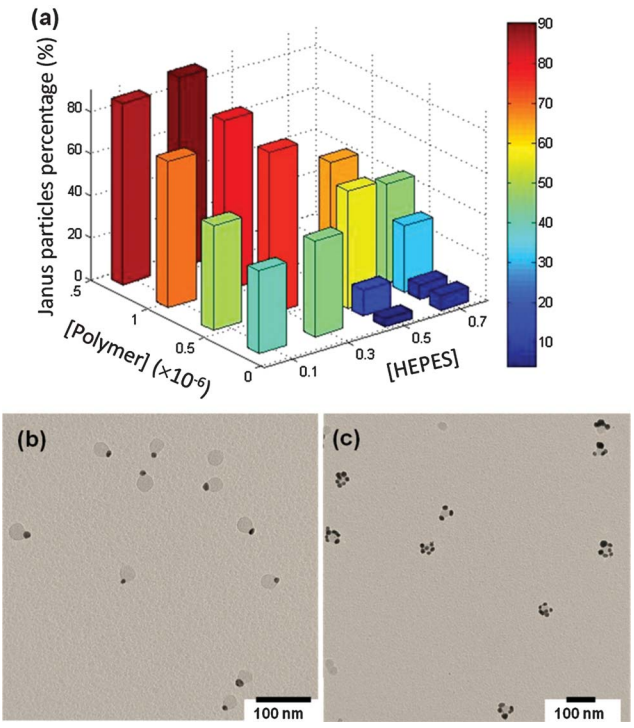

Fig. 3 (a) Statistical histogram of Au–micelle Janus nanoparticles and multi-particle clusters under different reaction conditions. The overall portion is changing with HEPES and micelles concentrations; (b) bright field TEM images of Janus nanoparticles; and (c) bright field TEM images of the raspberry-like Au–micelle hybrid, of which each micelle has multiple Au nanoparticles.

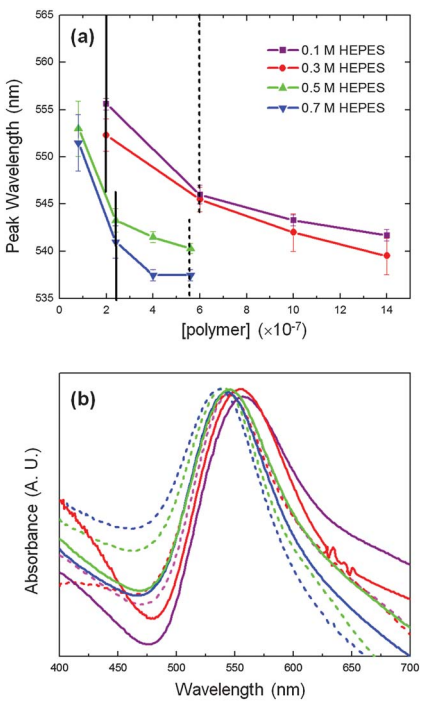

Fig. 4 (a) Shift of the average SPR peak wavelength of Au nanocrystals in the Au–micelle hybrid with micelle and HEPES concentrations. Points with different colors lying on the solid and dashed lines have the corresponding full UV-Vis spectra in (b). (b) Eight full UV-Vis spectra curves according to the peak wavelength lying in solid and dashed lines in (a), which clearly show the blue-shift of the dashed lines from the corresponding solid lines.

View Article Online

Published on 02 February 2012. Downloaded by University of Akron on 02/02/2015 19:01:47.

is able to influence the relative rates of the two independent processes of nucleation and growth of the metal particles.[40,52] As the HEPES concentration is increasing, the available gold is divided into more and more nuclei to make a difference in nanoparticle diameters. In dilute HEPES solution ($\leq$0.3 mol L^{-1}), existing gold particles are divided into fewer nuclei and the high micelle content is necessary for maintaining a high level of a single Au nanocrystal within a micelle. When the polymer concentration is low ($\leq 2.0 \times 10^{-7}$ mol L^{-1}), gold particle aggregates form readily, which can result in red shift of λ_{max}. When the HEPES concentration is high ($\geq$0.5 mol L^{-1}), there will be a larger number of nuclei and the corresponding Au nanoparticle size will be smaller. In those cases, when the polymer concentration is low ($\leq 2.4 \times 10^{-7}$ mol L^{-1}), instead of forming aggregates, each micelle can induce several Au nanoparticles representing raspberry-like morphology. The SPR is red-shifted to a higher wavelength and is due to the reduced nanoparticle interspacing.[49,52] In the window separated by both dashed and solid lines, with the same micelle content, λ_{max} is sharply blue shifted towards 530 nm as the HEPES concentration is increased, which also suggests that the size of Au nanocrystals is getting smaller and more uniform. Full UV-visible spectrophotometry curves with the λ_{max} on the solid and dashed lines in Fig. 4a are correspondingly present in Fig. 4b. The set of dashed lines are entirely blue shifted from the solid ones with the same color.

Conclusions

We have demonstrated a new aqueous route to synthesize hybrid nanostructures with a reduced symmetry that is scalable. Core–shell micelles function as a template to incubate Au nanoparticles *via* the relative volume fraction of PEO. Morphologies of Au–micelle nanoparticles can be changed from the Janus structure to the raspberry-like structure by adjusting the concentrations of micelle and HEPES buffer which functions as the reducing agent. The anisotropic structures were evident in TEM images, which statistically show that the optimal conditions to maximize Janus particlesare more favored when the micelle content is high while the HEPES concentration is low. Controlling nucleation and growth of inorganic structure with organic matrix is one of the fundamental processes for manipulating mineral deposition into microstructures. In recent years, a significant effort has been devoted to controllably assemble AuNPs with a defined stoichiometry, which enable the rational design of nanostructures with novel optical properties.[53–55] Using polymer assemblies as templates to synthesize AuNPs is one way to manipulate small assemblies of hybrid nanoparticles. Patterning Au nanoparticles using the polymer template is relatively cost-effective and has potentially wide applications. Due to the simplicity of our process, this method has a great potential for large-scale production. One of the promising applications is the fabrication of polymer–Au particles as label-free nanoprobes which possess the ability to sense and detect biomolecular signalling events inside and surrounding living cells.[4] When functionalized with targeting agents, the hybrid nanoparticle can function as plasmonic optical antennas which enhance molecular spectral information. Based on the concept, the drug delivery system with bioimaging agent can also be potentially realized.[56] Many gold nanostructures are being used in thermal ablation-based cancer therapy investigations.[57,58] A scalable route to well-defined structures will be critical as these types of materials advanced toward the clinic. We envision that our approach can be extended to different geometries and materials with the diversity of core–shell structures that are reported in the literature. This approach is a fast, more precise and economically feasible strategy that will afford the rational design and synthesis of complex Au nanoparticle superstructures. This strategy will also broaden the existing "bottom-up" fabrication strategies.

Acknowledgements

This work was supported by the Akron Functional Materials Center (AFMC) and The University of Akron Research Foundation. The authors acknowledge NSF-DMR-0821313 for providing the ESI-MS instrumentation for this research.

Notes and references

1 P. G. de Gennes, *Croat. Chem. Acta*, 1998, **71**(4), 833.
2 P. G. de Gennes, *Rev. Mod. Phys.*, 1992, **64**(3), 645.
3 F. Wurm and A. F. M. Kilbinger, *Angew. Chem., Int. Ed.*, 2009, **48**(45), 8412.
4 L. Y. Wu, B. M. Ross, S. Hong and L. P. Lee, *Small*, 2010, **6**(4), 503.
5 M. D. McConnell, M. J. Kraeutler, S. Yang and R. J. Composto, *Nano Lett.*, 2010, **10**, 603.
6 S. Hu and X. Gao, *J. Am. Chem. Soc.*, 2010, **132**, 7234.
7 S. Berger, A. Synytska, L. Ionov, K. Eichhorn and M. Stamm, *Macromolecules*, 2008, **41**(24), 9669.
8 C. Wang, H. Daimon and S. Sun, *Nano Lett.*, 2009, **9**(4), 1493.
9 S. Crossley, J. Faria, M. Shen and D. E. Resasco, *Science*, 2010, **327**, 68.
10 J. A. Champion, Y. K. Katare and S. Mitragotri, *Proc. Natl. Acad. Sci. U. S. A.*, 2007, **104**(29), 11901.
11 R. Langer and D. A. Tirrell, *Nature*, 2004, **428**, 487.
12 P. A. Suci, S. Kang, M. Young and T. Douglas, *J. Am. Chem. Soc.*, 2009, **131**, 9164.
13 Y. Li, W. Zhang, I. Hsieh, G. Zhang, Y. Cao, X. Li, C. Wesdemiotis, B. Lotz, H. Xiong and S. Z. D. Cheng, *J. Am. Chem. Soc.*, 2011, **133**, 10712.
14 V. N. Paunov and O. J. Cayre, *Adv. Mater.*, 2004, **16**, 788.
15 B. Wang, B. Li, B. Zhao and C. Y. Li, *J. Am. Chem. Soc.*, 2008, **130**, 11594.
16 Y. Yin, Y. Lu, B. Gates and Y. Xia, *J. Am. Chem. Soc.*, 2001, **123**, 8718.
17 Y. Yin, Y. Lu and Y. Xia, *J. Am. Chem. Soc.*, 2001, **123**, 771.
18 F. Wurm, H. M. Konig, S. Hilf and A. F. M. Kilbinger, *J. Am. Chem. Soc.*, 2008, **130**, 5876.
19 A. Walther, M. Hoffmann and A. H. E. Müller, *Angew. Chem., Int. Ed.*, 2008, **47**, 711.
20 D. Dendukuri and P. S. Doyle, *Adv. Mater.*, 2009, **21**, 4071.
21 S. Zhang, Z. Li, S. Samarajeewa, G. Sun, C. Yang and K. L. Wooley, *J. Am. Chem. Soc.*, 2011, **133**, 11046.
22 J. Yang, H. Elim, Q. Zhang, J. Y. Lee and W. Ji, *J. Am. Chem. Soc.*, 2006, **128**, 11921.
23 J. Ge, Y. Hu, T. Zhang and Y. Yi, *J. Am. Chem. Soc.*, 2007, **129**, 8974.
24 P. H. C. Camargo, Y. Xiong, L. Ji, J. M. Zhao and Y. Xia, *J. Am. Chem. Soc.*, 2007, **129**, 15452.
25 F. Wang, N. Phonthammachai, K. Y. Mya, W. W. Tjiu and C. Hu, *Chem. Commun.*, 2011, **47**, 767.
26 A. Ohnuma, E. C. Cho, P. H. C. Camargo, L. Au, B. Ohtani and Y. Xia, *J. Am. Chem. Soc.*, 2009, **131**, 1352.
27 S. Xing, Y. Feng, Y. Y. Tay, T. Chen, J. Xu, M. Pan, J. He, H. H. Hug, Q. Yan and H. Chen, *J. Am. Chem. Soc.*, 2010, **132**, 9537.
28 S. Yang, J. Xu, Z. Wang, H. Zeng and Y. Lei, *J. Mater. Chem.*, 2011, **21**, 11930.
29 L. Zhang and A. Eisenberg, *Polym. Adv. Technol.*, 1998, **9**, 677.
30 L. Y. Lin, N. S. Lee, J. Zhu, A. M. Nyström, D. J. Pochan, R. B. Dorshow and K. L. Wooley, *J. Controlled Release*, 2011, **152**, 37.

 This journal is © The Royal Society of Chemistry 2012

View Article Online

31 M. J. Joralemon, R. K. O'Reilly, C. J. Hawker and K. L. Wooley, *J. Am. Chem. Soc.*, 2005, **127**, 16892.
32 L. Zhang and A. Eisenberg, *Science*, 1996, **268**(5218), 1728.
33 C. Allen, J. Han, Y. Yu, D. Maysinger and A. Eisenberg, *J. Controlled Release*, 2000, **63**, 275.
34 Y. C. Cao, R. Jin and C. A. Mirkin, *Science*, 2002, **297**, 1536.
35 D. S. Seferos, D. A. Giljohann, H. D. Hill, A. E. Prigodich and C. A. Mirkin, *J. Am. Chem. Soc.*, 2007, **129**, 15477.
36 N. L. Rosi, D. A. Giljohann, C. S. Thaxton, A. K. R. Lytton-Jean, M. S. Han and C. A. Mirkin, *Science*, 2006, **312**, 1027.
37 D. Astruc, F. Lu and J. R. Aranzaes, *Angew. Chem., Int. Ed.*, 2005, **44**, 7852.
38 T. Chen, M. Yang, X. Wang, L. H. Tan and H. Chen, *J. Am. Chem. Soc.*, 2008, **130**, 11858.
39 C. Chen and N. L. Rosi, *Angew. Chem., Int. Ed.*, 2010, **49**, 1924.
40 S. K. Stanley, M. L. Becker, E. K. Lin and W. Wu, *Langmuir*, 2009, **25**(18), 10886.
41 J. Yu, M. L. Becker and G. A. Carri, *Small*, 2010, **6**(20), 2242.
42 X. Dong, W. Zhang, Y. Li, S. Zhang, M. Huang, R. P. Quirk and S. Z. D. Cheng, *Polym. Chem.*, 2011, in press.
43 P. Bhargava, J. X. Zheng, P. Li, R. P. Quirk, F. W. Harris and S. Z. D. Cheng, *Macromolecules*, 2006, **39**(14), 4880.
44 P. Bhargava, Y. Tu, J. X. Zheng, H. Xiong, R. P. Quirk and S. Z. D. Cheng, *J. Am. Chem. Soc.*, 2007, **129**, 1113.
45 P. Bhargava, J. X. Zheng, R. P. Quirk and S. Z. D. Cheng, *J. Polym. Sci., Part B: Polym. Phys.*, 2006, **44**(24), 3605.
46 L. Longenberger and G. Mills, *J. Phys. Chem.*, 1995, **99**(2), 475.
47 M. Iwamoto, K. Kuroda, V. Zaporojtchenko, S. Hayashi and F. Faupel, *Eur. Phys. J. E: Soft Matter Biol. Phys.*, 2003, **24**, 365.
48 T. Sakai and P. Alexandridis, *J. Phys. Chem. B*, 2005, **109**, 7766.
49 M. C. Deniel and D. Astruc, *Chem. Rev.*, 2004, **104**, 293.
50 I. Hussain, S. Graham, Z. Wang, B. Tan, D. C. Sherrington, S. P. Rannard, A. I. Cooper and M. Brust, *J. Am. Chem. Soc.*, 2005, **127**, 16398.
51 S. Link and M. A. EI-Sayed, *J. Phys. Chem. B*, 1998, **103**, 4212.
52 G. Frens, *Nature*, 1973, **241**, 20.
53 A. P. Alivisatos, K. P. Johnsson, X. Peng, T. E. Wilson, C. J. Loweth, M. P. Bruchez, Jr and P. G. Schultz, *Nature*, 1996, **382**(15), 609.
54 L. C. Brousseau, J. P. Novak, S. M. Marinakos and D. L. Feldheim, *Adv. Mater.*, 1999, **11**(6), 447.
55 C. J. Loweth, W. B. Caldwell, X. Gang, A. P. Alivisatos and P. G. Schultz, *Angew. Chem., Int. Ed.*, 1999, **38**(12), 1808.
56 D. Kim, S. Park, J. H. Lee, Y. Y. Jeong and S. Jon, *J. Am. Chem. Soc.*, 2007, **129**, 7661.
57 L. C. Kennedy, L. R. Bickford, N. A. Lewinski, A. J. Coughlin, Y. Hu, E. S. Day, J. L. West and R. A. Drezek, *Small*, 2011, **7**(2), 169–183.
58 K. Fu, J. Sun, L. R. Bickford, A. W. H. Lin, N. J. Halas, T. Yu and R. A. Drezek, *Nanotechnology*, 2008, **19**(4), 045103.

Published on 02 February 2012. Downloaded by University of Akron on 02/02/2015 19:01:47.